Atmos. Meas. Tech. Discuss., 7, 12219–12248, 2014
www.atmos-meas-tech-discuss.net/7/12219/2014/
doi:10.5194/amtd-7-12219-2014

Atmospheric Measurement Techniques Discussions

Low-level mixing height detection in coastal locations with a scanning Doppler lidar

V. Vakkari[1], E. J. O'Connor[1,2], A. Nisantzi[3], R. E. Mamouri[3], and D. G. Hadjimitsis[3]

[1]Finnish Meteorological Institute, Helsinki, Finland
[2]Meteorology Department, University of Reading, Reading, UK
[3]Cyprus University of Technology, Limassol, Cyprus

Received: 13 October 2014 – Accepted: 18 November 2014 – Published: 9 December 2014

Correspondence to: V. Vakkari (ville.vakkari@fmi.fi)

Published by Copernicus Publications on behalf of the European Geosciences Union.

Abstract

Mixing height is one of the key parameters in describing lower tropospheric dynamics, and capturing the diurnal variability is crucial, especially in interpreting surface observations. In this paper we introduce a method for identifying mixing heights below the vertical minimum range of a scanning Doppler lidar. The method we propose is based on velocity variance in low elevation angle conical scanning, and is applied to measurements in two very different coastal environments: Limassol, Cyprus during summer; and Loviisa, Finland during winter. At both locations, the new method agrees well with mixing heights derived from turbulent kinetic energy dissipation rate profiles obtained from vertically-pointing measurements. The low-level scanning routine frequently indicated non-zero mixing heights less than 100 m above the surface. Such low mixing heights were more common at wintertime Loviisa on the Baltic Sea coast than during summertime in Mediterranean Limassol.

1 Introduction

Mixing is a key process in the lower troposphere for climate, weather and air quality. Turbulent mixing is regarded as a significant player in aerosol microphysical processes (e.g. Nilsson et al., 2001; Wehner et al., 2010; Hirsikko et al., 2013) and in cloud microphysics (e.g. Pinsky et al., 2008). To represent turbulent mixing in numerical models requires an understanding of the variability in space and time, the length scales involved, and the processes that are responsible: friction, surface heating, shear (Baklanov et al., 2011). Stable layers and diurnal cycles require particular attention (Holtslag et al., 2013). From an air quality perspective, the height of the layer that is in constant contact with the surface, i.e. mixing layer height, MLH, is a critical parameter governing the dispersion of air pollutants (e.g. White et al., 2009). The continuous monitoring of the atmospheric mixing profile covering the lowest few kilometres is not a straightforward task and there are only a few long-term data sets (e.g. Harvey et al., 2013;

AMTD
7, 12219–12248, 2014

Schween et al., 2014). In many studies the mixed layer is characterised indirectly, often in terms of mixing height inferred from aerosol backscatter profiles (e.g. Baars et al., 2008; Korhonen et al., 2014) or temperature profiles (e.g. Beyrich and Leps, 2012). However, indirect methods in mixing height estimation may potentially suffer from erroneous interpretation, especially for stable layers, and during the initial early morning phase or afternoon collapse of a convective boundary layer (e.g. Pearson et al., 2010; Schween et al., 2014).

In-situ measurements of turbulent mixing in the lower troposphere have been conducted successfully on a variety of platforms. For instance, turbulent mixing measurements have been carried out with radiosondes (Harrison and Hogan, 2006), tethered balloons (Siebert et al., 2003), various aircraft (Muschinski and Wode, 1998; Khelif et al., 1999) and recently, small unmanned aerial vehicles (Martin et al., 2011). Deployed in-aircraft in-situ sensors can yield mixing information with an unsurpassed resolution both spatially and temporally (Muschinski and Wode, 1998; Martin et al., 2014). The drawback with these methods is that they are restricted to short-term campaigns. Only radiosonde measurements are possible routinely, but turbulent sensors are not yet part of the standard operational package. Furthermore, the temporal resolution for routine operational launches is rather coarse; typically a maximum of four per day. Mast-based sonic anemometers provide excellent turbulent measurements with high temporal resolution, but masts taller than 100 m are rare; therefore remote sensing techniques are currently the only viable option for long-term continuous monitoring through the entire lower troposphere.

Several remote sensing techniques, such as Doppler sodar (e.g. Beyrich, 1997; Seibert et al., 2000; Emeis et al., 2008), Doppler lidar (e.g. Harvey et al., 2013; Schween et al., 2014) and radar windprofiler (e.g. Bianco et al., 2008; Emeis et al., 2008), enable continuous measurements of the vertical wind velocity, w, profile with high time resolution. Subsequently, these measurements can be processed to provide vertical profiles of vertical velocity variance, σ_w^2 (e.g. Pearson et al., 2010), or turbulent kinetic energy dissipation rate (e.g. O'Connor et al., 2010) with resolutions better than a few

AMTD
7, 12219–12248, 2014

minutes. However, no single remote sensing instrument has been able to cover the full range of turbulent mixing heights from instrument level up to the top of the atmospheric boundary layer. Doppler sodars can cover the low range from 10 m up to a few hundred metres, possibly reaching 1 km in good conditions (e.g. Emeis et al., 2008), but, in many environments, the daytime convective mixing height exceeds the range of sodars. On the other hand, vertically-pointing Doppler lidars and radar windprofilers are usually sensitive enough to reach the top of the atmospheric boundary layer, and beyond, but cannot see closer than an instrument-specific range; typically 100–200 m (Bianco et al., 2008; Pearson et al., 2009; Srinivasulu et al., 2012), which hampers the detection of low-level mixing.

Scanning Doppler lidars can partially overcome a minimum height limitation by retrieving radial wind velocity measurements at a low elevation angle (Banta et al., 2006). In this paper we present a method whereby scanning Doppler lidars can identify the presence of turbulent mixing from the instrument level up, making it possible to cover the full range of mixing heights with an appropriate selection of scan types from one instrument. From the various possible low-elevation angle scanning patterns, we selected vertical azimuth display (VAD) scans as the basis for low-level mixing height detection. The main reason for choosing VAD scans is that it simultaneously provides the horizontal wind profile (e.g. Browning and Wexler, 1968) and can be utilised in studying the surface effects on the wind field in the vicinity of the Doppler lidar. The method for identifying turbulent mixing and obtaining mixing level heights is described in Sect. 2. By applying the VAD-based mixing height detection to two data sets from very different environments, i.e. summertime Mediterranean coast and wintertime Baltic Sea coast, in Sect. 3, we show that this method compares well with mixing height inferred from vertically-pointing measurements. With this method we frequently identified mixing heights below the lowest usable range gate of the Doppler lidar in vertical mode at both locations.

AMTD
7, 12219–12248, 2014

2 Methodology

2.1 Measurements

In this study we utilise Doppler lidar measurements from two locations: Limassol in Cyprus, and Loviisa in Finland as indicated in Fig. 1. Measurements were carried out with a Halo Photonics Streamline scanning Doppler lidar (Pearson et al., 2009). The Halo Photonics Streamline is a 1.5 µm pulsed Doppler lidar with a heterodyne detector that can switch between co- and cross-polar channels (Pearson et al., 2009). Standard operating specifications are given in Table 1, and the minimum range of the instrument was 90 m. The accumulation time per ray varied according to scan type and location.

At Limassol, measurements were performed at the Cyprus University of Technology campus (34.6756° N, 33.0403° E, 15 m a.s.l.) from 22 August to 15 October 2013. Solar noon at Limassol is 09:40 UTC. The measurement site was on a roof top 600 m NE from the Mediterranean Sea shoreline (Fig. 1). The Limassol campaign took place in typical Mediterranean summer conditions with surface temperatures ranging from +15 to +35 °C, very low cloud cover and three rain showers.

At Loviisa, the measurement campaign took place on the Fortum Power and Heat Oy nuclear power plant site on Hästholmen island (60.3660° N, 26.3500° E, 24 m a.s.l.) from 10 December 2013 to 17 March 2014. Solar noon at Loviisa is 10:20 UTC. Hästholmen island is approximately 2000 m long in the SE–NW direction and 500 m wide in the SW–NE direction (Fig. 1). From the measurement platform at the centre of the island, the distance to shoreline in the SW direction was 300 m, and in the NE direction, 200 m. The Loviisa measurements were representative of winter conditions in the Baltic Sea region, characterised by surface temperatures ranging from –25 to +10 °C, frequent bursts of rain and snow, and few cloud-free conditions.

At both locations, a fixed scanning routine was operated continuously throughout the campaign. At Limassol the scanning schedule consisted of two VAD scans (e.g. Browning and Wexler, 1968) at 30 and 10° elevation angle every 20 min (Table 2), a three beam Doppler beam swing (DBS) every 20 min, and a range height indicator

AMTD
7, 12219–12248, 2014

(RHI) scan every 10 min. Besides scanning, 15 out of every 20 min were available for vertically-pointing measurements. Vertically pointing data was recorded at 3 s integration time and every second beam was measured with the cross-polar receiver (Pearson et al., 2009).

At Loviisa, the terrain allowed VAD scans to be operated at a lower elevation angle than at Limassol and thus the scan schedule at Loviisa consisted of a 24-point VAD scan at 15° elevation angle and a 72-point VAD scan at 4° elevation angle (Table 2). At Loviisa, vertically-pointing measurements were initially operated at 8 s integration time but on 11 February 2014 the integration time was increased to 16 s. Again, every second vertical beam was measured with the cross-polar receiver as at Limassol. Due to the longer integration time for each beam when scanning, there were 13 min free per 30 min for vertically-pointing measurements. At both locations the focus of the Doppler lidar telescope was set to 2000 m. In this study we utilise only the VAD scans and co-polar vertically-pointing measurements.

Velocity measurement uncertainty is directly related to the instrument sensitivity, so there is a potential trade-off between achieving the high temporal resolution suitable for investigating turbulent conditions at the expense of measurement sensitivity and uncertainty. The integration times for each particular scan at each location were selected to achieve the highest temporal resolution possible while retaining sufficient sensitivity for each individual measurement; at Loviisa, a much lower atmospheric aerosol loading required a longer integration time per individual ray. Additional optimisation was required when implementing the scan schedule so that the relevant scans were acquired while still providing enough vertically-pointing coverage.

2.2 Estimating turbulent mixing from a VAD

In a smooth homogeneous wind flow field, radial velocities in a VAD follow a sinusoidal curve. A vertical profile of the horizontal wind vector is obtained from the sinusoidal fit (Fig. 2a) to the VAD at each elevation level (Browning and Wexler, 1968). Deviations from this ideal shape (Fig. 2a) can originate from several processes such as wind

AMTD
7, 12219–12248, 2014

field divergence or deformation (Browning and Wexler, 1968), instrumental noise and turbulence. Considering one radial measurement in a VAD, the observed radial velocity (V_R) at a single range gate contains the following potential contributions:

$$V_R = V_{wind} + V_{turb} + V_{def} + V_{div} + V_{surf} + \delta\,, \quad (1)$$

where V_{wind} is the radial component of homogeneous horizontal wind, V_{turb} is the contribution from turbulent mixing that we are interested in, V_{def} is the deformation component, V_{div} is the divergence component, V_{surf} is the deviation from ideal because of surface interactions, such as wind flow around a building, and δ is the instrumental measurement uncertainty.

The horizontal wind component V_{wind} in Eq. (1) is estimated by fitting a sinusoidal curve to V_R (Fig. 2a) at each elevation level in a VAD. Thus the fitting procedure provides $V_R = V_{wind} + R$ and R, the residual of the fit, is due to the departure from an ideal smooth homogeneous wind field:

$$R = V_{turb} + V_{def} + V_{div} + V_{surf} + \delta\,. \quad (2)$$

In order to extract the atmospheric turbulent mixing information from this residual, the non-turbulent contributions have to be obtained or estimated. In quiescent conditions, the terms V_{def}, V_{div} and V_{surf} in (2) may form most of the residual. This is evident when correlating the residuals of two consecutive range gates as in Fig. 2b; a high correlation indicates that the residuals are dominated by flow patterns in a length scale that is large compared to the 30 m radial resolution of the instrument.

Of the non-turbulent terms in (2), δ can be calculated from the measurements (Pearson et al., 2009), and in principle, V_{def} and V_{div} can be estimated by fitting higher-order harmonic terms to V_R (Browning and Wexler, 1968). However, quantifying the surface interactions responsible for V_{surf} would require such detailed knowledge of the surface at the measurement location that it makes it impractical to determine V_{turb} directly from Eq. (2).

AMTD
7, 12219–12248, 2014

Therefore, we consider the change in V_R from one range gate at distance r to the next range gate at $r + 30\,\mathrm{m}$ for one radial measurement:

$$V_R(r) - V_R(r + 30\,\mathrm{m}) = \Delta V_R = \Delta V_{wind} + \Delta R. \quad (3)$$

Note that in this approach it is vital to account for the vertical profile of horizontal wind, i.e. ΔV_{wind} calculated from the two successive sinusoidal fits. The wind profile cannot be neglected even if the change in altitude between the two consecutive VAD elevation levels is only 5 m. This is evident as a relatively high correlation between ΔV_R and ΔV_{wind}, as demonstrated in Fig. 2c for one VAD scan at Limassol.

Expanding the change in residual term in (3) we have

$$\Delta R = \Delta V_{turb} + \Delta V_{def} + \Delta V_{div} + \Delta V_{surf} + \upsilon\,, \quad (4)$$

where

$$\upsilon = \sqrt{\delta(r)^2 + \delta(r + 30\,\mathrm{m})^2}\,, \quad (5)$$

i.e. we have assumed that the instrumental measurement uncertainty for the two range gates is uncorrelated. Deformation and divergence are assumed to occur over length scales that are significantly larger than the Doppler lidar range resolution of 30 m (e.g. Browning and Wexler, 1968) and therefore we state here:

$$V_{def}(r) \approx V_{def}(r + 30\,\mathrm{m}); \Delta V_{def} \approx 0\,; \quad (6a)$$

$$V_{div}(r) \approx V_{div}(r + 30\,\mathrm{m}); \Delta V_{div} \approx 0\,. \quad (6b)$$

Similarly, if the surface is homogeneous or the measurement is not close to the surface, then the surface contribution term is assumed to be either negligible or not expected to change at the lidar range resolution scale, i.e.

$$V_{surf}(r) \approx V_{surf}(r + 30\,\mathrm{m}); \Delta V_{surf} \approx 0\,. \quad (7)$$

AMTD
7, 12219–12248, 2014

With these assumptions we can now estimate

$$\Delta R \approx \Delta V_{\text{turb}} + \upsilon\,. \tag{8}$$

Thus the proxy variable for identifying turbulent mixing is the variance of the difference of residuals from two consecutive elevation levels in a VAD,

$$\sigma^2_{\text{VAD}}(r + 15\,\text{m}) = \frac{1}{n}\sum_{i=1}^{n}\left(\Delta R_i - \frac{1}{n}\sum_{i=1}^{n}(\Delta R_i)\right)^2 - \sigma^2_{\upsilon}\,, \tag{9}$$

where the subscript i refers to individual radials and n is the number of radials within a VAD. The measurement uncertainty variance σ^2_{υ} is estimated from the δ^2_i calculated for every ith radial:

$$\sigma^2_{\upsilon} = \text{median}\left(\delta(r)^2\right) + \text{median}\left(\delta(r + 30\,\text{m})^2\right), \tag{10}$$

where median is taken over all radials at each range gate.

The instrument uncertainty in velocity is a function of the signal-to-noise ratio, SNR, (Pearson et al., 2009) and is calculated for every individual point in a VAD. The choice of median in (10) is to avoid outliers skewing the distribution. In general, most of the points in a particular VAD display similar sensitivity, but the presence of cloud or precipitation can increase SNR, whereas certain radials may be completely or partially obscured by buildings or trees. Here, we only calculate σ^2_{VAD} when SNR > 0.0025 for at least 20 out of 24 points at any given elevation level. In terms of σ^2_{υ} this is equivalent to a threshold of $1.58\,\text{m}^2\,\text{s}^{-2}$ using the instrument specifications given in Table 1.

Abrupt changes in surface roughness also have an impact on the turbulent properties of the wind field (Garrat, 1990). For instance the 4° elevation angle VAD at Loviisa is so close to the surface that the radial wind field is clearly affected by the change of surface roughness moving from sea to land. To minimise the effect of surface roughness changes at Loviisa we considered only a 55° wide sector (i.e. 12 azimuthal directions) upwind of the island to derive mixing height from the 4° elevation angle VAD.

AMTD
7, 12219–12248, 2014

2.3 Turbulent kinetic energy dissipation rate

The dissipation rate of turbulent kinetic energy (TKE) was determined from the vertical velocity measurements according to the method described by O'Connor et al. (2010). This method utilises the velocity variance over a specific number of samples, from which the dissipation rate is derived using appropriate advective length scales obtained from the vertical profiles of horizontal wind. The implicit constraint in this method is that the advective length scales for calculating the variance should remain within the inertial subrange. Typically, this means that the total time available for collecting samples for one variance profile should not exceed about three minutes and that the number of samples available per dissipation rate profile therefore depends on the integration time for an individual ray. For vertical profiles with three minute resolution at Limassol, optimal operating conditions provided 60 vertical velocity samples per dissipation rate profile. At Loviisa, a much lower atmospheric aerosol loading required a longer integration time per individual ray to obtain sufficient sensitivity; therefore only 11 vertical velocity samples per three-minute resolution dissipation rate profile were available. Vertical resolution was 30 m, and dissipation rate values were determined only when the relative uncertainty in the variance was less than 1, i.e. observed variance at least twice the theoretical contribution from noise.

3 Results and discussion

3.1 Comparison to vertical wind speed variance

We first investigate how σ^2_{VAD} correlates with the vertical velocity variance σ^2_{w} calculated directly from the vertically-pointing time series. Note that we do not expect σ^2_{VAD} to be equivalent to σ^2_{w} since the effective measurement volumes can encompass very different length scales. Figure 3 shows that, at Limassol, σ^2_{VAD} from both 30° and 10° elevation VADs correlates reasonably well with σ^2_{w}. At Loviisa the correlation is not

AMTD
7, 12219–12248, 2014

quite as good for the 15° VAD (Fig. 3). However, the relationship between σ^2_{VAD} and σ^2_w is reasonably linear especially for $\sigma^2_w < 0.1\,m^2\,s^{-2}$ (Fig. 3), which is the most important range for determining the top of the mixing layer. The relationship between σ^2_{VAD} and σ^2_w also appears to be independent of the VAD elevation angle (Fig. 3) and thus σ^2_{VAD} can be used as a proxy for turbulent mixing.

3.2 Comparing mixing height from a VAD and vertically-pointing measurements

The diurnal variation of TKE dissipation rate calculated from vertically-pointing measurements is plotted together with σ^2_{VAD} for Limassol in Figs. 4 and 5, and for Loviisa in Figs. 6 and 7. In a qualitative sense the diurnal dissipation rate and σ^2_{VAD} profiles agree. The greatest difference is the instrument sensitivity for VADs below 15° in elevation; the signal clearly peters out at a lower altitude than for the vertically-pointing data. This is due to two reasons: at low elevation angles, the range, or path-length, to a given altitude is obviously much further than when vertically-pointing and the relative rate of attenuation in the vertical plane is correspondingly higher; the integration time for vertically-pointing rays can be increased without a major impact on the scan schedule.

We used the simplest possible mixing layer height detection scheme – a constant threshold value – to assess the usefulness of σ^2_{VAD} as a measure of the top of the mixing layer. For σ^2_{VAD}, the top of the mixing layer was diagnosed as the altitude where σ^2_{VAD} first drops below $0.05\,m^2\,s^{-2}$. A threshold dissipation rate of $10^{-4}\,m^2\,s^{-3}$ (O'Connor et al., 2010) was selected for the vertically-pointing data. In Figs. 4–7, a mixing layer height estimate is given only if there is more data above, i.e. no mixing layer height estimate is given if the highest data point, dissipation rate or σ^2_{VAD}, is still above the respective threshold. However, in such cases (e.g. Fig. 4c) the highest data point can be used as a lower bound for the mixing height.

AMTD
7, 12219–12248, 2014

Mixing layer heights obtained in this manner from the dissipation rate and σ^2_{VAD} profiles are in good agreement as seen in Figs. 4–7. What is more, the σ^2_{VAD} profile can be used to check whether the mixed regions observed in the vertically pointing data are indeed connected to the surface. For instance, Limassol vertically-pointing data indicates a mixed-layer up to 500 m at 00:30 UTC on 24 August 2013, but σ^2_{VAD} from the 10° VAD shows that this turbulent region is not connected to the surface. In fact, based on the horizontal wind profile obtained from the VADs, this turbulent region lies at the lower edge of a low-level jet.

A comparison of mixing layer top obtained from TKE dissipation rate and 30° elevation angle σ^2_{VAD} for the full length of the campaign at Limassol (Fig. 8) shows a reasonable agreement between the two methods. However, as the VAD radius increases up to 400 m and above, the comparison becomes poorer. This behaviour can be expected considering that the correlation length scale of turbulence typically scales with mixing height (e.g. Lothon et al., 2009). In Fig. 8 the comparison is plotted for the nearest neighbour TKE dissipation rate for each VAD based mixing height estimate.

The connection of correlation length scale and mixing height renders comparison of mixing heights from vertically-pointing measurements and lower elevation angle VADs unfeasible as the radii of 10 and 15° elevation angle VADs already exceed 500 m at the lowest usable range in the vertical at Limassol and Loviisa (Table 3). However, despite the large radius the 10 and 15° elevation angle VAD based mixing heights agree reasonably well with the vertically-pointing measurements at the lowest vertically-pointing range gate (Table 3).

The 4° elevation angle VAD at Loviisa is so close to the surface that the change of surface roughness from land to sea can have a major effect on σ^2_{VAD}. To minimise the effects of local topography we have only calculated σ^2_{VAD} from the VAD at 4° elevation angle for a 55° wide sector (i.e. 12 azimuthal angles) upwind of the lidar. Then, the σ^2_{VAD} from the 4° elevation angle VAD agrees reasonably well with σ^2_{VAD} from the 15° elevation angle VAD at Loviisa (Figs. 6 and 7). Mixing heights from 4 and 15° elevation angle VADs also compare well for the lower altitudes of the 15° elevation angle VAD

AMTD
7, 12219–12248, 2014

(Table 3). The width of the 55° azimuthal sector for the 4° elevation angle VAD mixing height calculation is 410 m at the elevation of the lowest gate of the 15° elevation angle VAD.

3.3 Frequency of low mixing level heights at Limassol and Loviisa

The vertically-pointing dissipation rate data close to surface indicates no significant mixing, implying mixing-level heights below the lowest vertical gate, 42 % of the time at Limassol and 62 % of the time at Loviisa. The VAD-based mixing height estimates show that, at Limassol, in 58 % of the cases when mixing level height must be below the vertically-pointing altitude limit, there is a shallow mixed layer at the surface (Fig. 9). At Loviisa the VADs indicate a shallow mixed layer at the surface on 87 % of the cases when the mixing level height must be below the vertically-pointing altitude limit (Fig. 9).

At Limassol mixing level heights exhibit a clear diurnal cycle with low-altitude mixing levels occurring almost exclusively during night time (Fig. 9b). This agrees with radiosonde observations of mixing level heights at coastal Mediterranean locations during summer (e.g. Seidel et al., 2012). At Loviisa, on the other hand, very low mixing heights are also common during daytime (Fig. 9d), typical for cold conditions with a stably-stratified atmosphere and minimal surface heating (e.g. Liu and Liang, 2010).

4 Conclusion

We have shown for two very different environments that a low elevation angle Doppler lidar VAD scan can be used to identify the presence of turbulent mixing in the atmosphere. Furthermore, the VAD-based proxy for turbulence can be used to identify the mixing height. If scanning at a very low elevation angle is feasible at the measurement location, the VAD-based mixing level height can detect the presence or absence of mixing from the instrument level up. However, at elevation angles lower than 10°,

AMTD
7, 12219–12248, 2014

the impact of surface roughness changes across the VAD volume must be taken into consideration.

Comparison of mixing heights from vertically-pointing data and VADs shows reasonably good agreement, especially considering the simplicity of the mixing height detection scheme used here. However, the rapid increase in radius for VADs at low elevation angles limits the altitude range of mixing height retrievals from VADs. Therefore, to cover the full range of mixing heights from ground level up, a combination of vertically-pointing and VAD measurements are most suitable. In this manner, turbulent mixing can be identified from the surface up to heights of a kilometre or more continuously with a good time resolution. At the same time, VADs can be used to retrieve the wind profile, which in turn can be used to e.g. identify wind shear generated mixing.

Finally we have demonstrated that very shallow mixing layers can be present during the majority of the time that vertically-pointing measurements indicate no mixing; i.e. mixing height is below the lowest measurement at vertical. At Limassol, representing Mediterranean summer time conditions, such low mixing heights occurred only during the night: at Loviisa, in Baltic Sea winter time conditions, very low mixing heights were also common during the day.

Acknowledgements. We gratefully acknowledge the financial support by the Nessling foundation (grant 2013006) as well as the support of Fennovoima Oy, Fortum Power and Heat Oy and Teollisuuden Voima Oyj under a joint research project. This work was co-funded by the European Regional Development Fund and the Republic of Cyprus through the Research Promotion Foundation (PENEK/0311/05).

References

Baars, H., Ansmann, A., Engelmann, R., and Althausen, D.: Continuous monitoring of the boundary-layer top with lidar, Atmos. Chem. Phys., 8, 7281–7296, doi:10.5194/acp-8-7281-2008, 2008.

AMTD
7, 12219–12248, 2014

Baklanov, A. A., Grisogono, B., Bornstein, R., Mahrt, L., Zilitinkevich, S. S., Taylor, P., Larsen, S. E., Rotach, M. W., and Fernando, H. J. S.: The nature, theory, and modeling of atmospheric planetary boundary layers, B. Am. Meteorol. Soc., 92, 123–128, 2011.

Banta, R. M., Pichugina, Y. L., and Brewer, W. A.: Turbulent velocity-variance profiles in the stable boundary layer generated by a nocturnal low-level jet, J. Atmos. Sci., 63, 2700–2719, doi:10.1175/JAS3776.1, 2006.

Beyrich, F.: Mixing height estimation from sodar data – a critical discussion, Atmos. Environ., 31, 3941–3953, doi:10.1016/S1352-2310(97)00231-8, 1997.

Beyrich, F. and Leps, J.-P.: An operational mixing height data set from routine radiosoundings at Lindenberg: methodology, Meteorol. Z., 21, 337–348, doi:10.1127/0941-2948/2012/0333, 2012.

Bianco, L., Wilczak, J. M., and White, A. B.: Convective boundary layer depth estimation from wind profilers: statistical comparison between an automated algorithm and expert estimations, J. Atmos. Ocean. Tech., 25, 1397–1413, doi:10.1175/2008JTECHA981.1, 2008.

Browning, K. A. and Wexler, R.: The determination of kinematic properties of a wind field using Doppler radar, J. Appl. Meteorol., 7, 105–113, doi:10.1175/1520-0450(1968)007<0105:TDOKPO>2.0.CO;2, 1968.

Emeis, S., Schaefer, K., and Muenkel, C.: Surface-based remote sensing of the mixing-layer height – a review, Meteorol. Z., 17(5), 621–630, doi:10.1127/0941-2948/2008/0312, 2008.

Garrat, J. R.: The internal boundary layer – a review, Bound.-Lay. Meteorol., 50, 171–203, 1990.

Harrison, R. G. and Hogan, R. J.: In situ atmospheric turbulence measurement using the terrestrial magnetic field – a compass for a radiosonde, J. Atmos. Ocean. Tech., 23, 517–523, doi:10.1175/JTECH1860.1, 2006.

Harvey, N. J., Hogan, R. J., and Dacre, H. F.: A method to diagnose boundary-layer type using Doppler lidar, Q. J. Roy. Meteor. Soc., 139, 1681–1693, doi:10.1002/qj.2068, 2013.

Hirsikko, A., O'Connor, E. J., Komppula, M., Korhonen, K., Pfüller, A., Giannakaki, E., Wood, C. R., Bauer-Pfundstein, M., Poikonen, A., Karppinen, T., Lonka, H., Kurri, M., Heinonen, J., Moisseev, D., Asmi, E., Aaltonen, V., Nordbo, A., Rodriguez, E., Lihavainen, H., Laaksonen, A., Lehtinen, K. E. J., Laurila, T., Petäjä, T., Kulmala, M., and Viisanen, Y.: Observing wind, aerosol particles, cloud and precipitation: Finland's new ground-based remote-sensing network, Atmos. Meas. Tech., 7, 1351–1375, doi:10.5194/amt-7-1351-2014, 2014.

AMTD
7, 12219–12248, 2014

Holtslag, A. A. M., Svensson, G., Baas, P., Basu, S., Beare, B., Beljaars, A. C. M., Bosveld, F. C., Cuxart, J., Lindvall, J., Steeneveld, G. J., Tjernström, M., and Van De Wiel, B. J. H.: Stable atmospheric boundary layers and diurnal cycles: challenges for weather and climate models, B. Am. Meteorol. Soc., 94, 1691–1706, 2013.

Khelif, D., Burns, S. P., and Friehe, C. A.: Improved wind measurements on research aircraft, J. Atmos. Ocean. Tech., 16, 860–875, doi:10.1175/1520-0426(1999)016<0860:IWMORA>2.0.CO;2, 1999.

Korhonen, K., Giannakaki, E., Mielonen, T., Pfüller, A., Laakso, L., Vakkari, V., Baars, H., Engelmann, R., Beukes, J. P., Van Zyl, P. G., Ramandh, A., Ntsangwane, L., Josipovic, M., Tiitta, P., Fourie, G., Ngwana, I., Chiloane, K., and Komppula, M.: Atmospheric boundary layer top height in South Africa: measurements with lidar and radiosonde compared to three atmospheric models, Atmos. Chem. Phys., 14, 4263–4278, doi:10.5194/acp-14-4263-2014, 2014.

Liu, S. and Liang, X.-Z.: Observed diurnal cycle climatology of planetary boundary layer height, J. Climate, 23, 5790–5809, doi:10.1175/2010JCLI3552.1, 2010.

Lothon, M., Lenschow, D., and Mayor, S.: Doppler lidar measurements of vertical velocity spectra in the convective planetary boundary layer, Bound.-Lay. Meteorol., 132, 205–226, doi:10.1007/s10546-009-9398-y, 2009.

Martin, S., Bange, J., and Beyrich, F.: Meteorological profiling of the lower troposphere using the research UAV "M^2AV Carolo", Atmos. Meas. Tech., 4, 705–716, doi:10.5194/amt-4-705-2011, 2011.

Martin, S., Beyrich, F., and Bange, J.: Observing entrainment processes using a small unmanned aerial vehicle: a feasibility study, Bound.-Lay. Meteorol., 150(3), 449–467, doi:10.1007/s10546-013-9880-4, 2014.

Muschinski, A. and Wode, C.: First in situ evidence for coexisting submeter temperature and humidity sheets in the lower free troposphere, J. Atmos. Sci., 55, 2893–2906, doi:10.1175/1520-0469(1998)055<2893:FISEFC>2.0.CO;2, 1998.

National Land Survey of Finland, Elevation model 10 m, http://www.maanmittauslaitos.fi/en/NLS_open_data_licence_version1_20120501, last access: 2 October 2014.

Nilsson, E. D., Rannik, Ü., Kulmala, M., Buzorius, G., and O'Dowd, C. D.: Effects of continental boundary layer evolution, convection, turbulence and entrainment, on aerosol formation, Tellus B, 53, 441–461, doi:10.1034/j.1600-0889.2001.530409.x, 2001.

AMTD
7, 12219–12248, 2014

O'Connor, E. J., Illingworth, A. J., Brooks, I. M., Westbrook, C. D., Hogan, R. J., Davies, F., and Brooks, B. J.: A method for estimating the turbulent kinetic energy dissipation rate from a vertically pointing Doppler lidar, and independent evaluation from balloon-borne in situ measurements, J. Atmos. Ocean. Tech., 27, 1652–1664, doi:10.1175/2010JTECHA1455.1, 2010.

Pearson, G., Davies, F., and Collier, C.: An analysis of the performance of the UFAM pulsed Doppler lidar for observing the boundary layer, J. Atmos. Ocean. Tech., 26, 240–250, doi:10.1175/2008JTECHA1128.1, 2009.

Pearson, G., Davies, F., and Collier, C.: Remote sensing of the tropical rain forest boundary layer using pulsed Doppler lidar, Atmos. Chem. Phys., 10, 5891–5901, doi:10.5194/acp-10-5891-2010, 2010.

Pinsky, M., Khain, A., and Krugliak, H.: Collisions of cloud droplets in a turbulent flow. Part 5: Application of detailed tables of turbulent collision rate enhancement to simulation of droplet spectra evolution, J. Atmos. Sci., 65, 357–374, doi:10.1175/2007JAS2358.1, 2008.

Schween, J. H., Hirsikko, A., Löhnert, U., and Crewell, S.: Mixing-layer height retrieval with ceilometer and Doppler lidar: from case studies to long-term assessment, Atmos. Meas. Tech., 7, 3685–3704, doi:10.5194/amt-7-3685-2014, 2014.

Seibert, P., Beyrich, F., Gryning, S.-E., Joffre, S., Rasmussen, A., and Tercier, P.: Review and intercomparison of operational methods for the determination of the mixing height, Atmos. Environ., 34(7), 1001–1027, doi:10.1016/S1352-2310(99)00349-0, 2000.

Seidel, D. J., Zhang, Y., Beljaars, A., Golaz, J.-C., Jacobson, A. R., and Medeiros, B.: Climatology of the planetary boundary layer over the continental United States and Europe, J. Geophys. Res.-Atmos., 117, D17106, doi:10.1029/2012JD018143, 2012.

Siebert, H., Wendisch, M., Conrath, T., Teichmann, U., and Heintzenberg, J.: A new tethered balloon-borne payload for fine-scale observations in the cloudy boundary layer, Bound.-Lay. Meteorol., 106, 461–482, doi:10.1023/A:1021242305810, 2003.

Srinivasulu, P., Yasodha, P., Kamaraj, P., Rao, T. N., Jayaraman, A., Reddy, S. N., and Satyanarayana, S.: 1280-MHz active array radar wind profiler for lower atmosphere: system description and data validation, J. Atmos. Ocean. Tech., 29, 1455–1470, doi:10.1175/JTECH-D-12-00030.1, 2012.

United States Geological Survey, Global Multi-resolution Terrain Elevation Data 2010, available at: http://earthexplorer.usgs.gov/, last access: 2 October 2014.

AMTD
7, 12219–12248, 2014

Wehner, B., Siebert, H., Ansmann, A., Ditas, F., Seifert, P., Stratmann, F., Wiedensohler, A., Apituley, A., Shaw, R. A., Manninen, H. E., and Kulmala, M.: Observations of turbulence-induced new particle formation in the residual layer, Atmos. Chem. Phys., 10, 4319–4330, doi:10.5194/acp-10-4319-2010, 2010.

White, J. M., Bowers, J. F., Hanna, S. R., and Lundquist, J. K.: Importance of using observations of mixing depths in order to avoid large prediction errors by a transport and dispersion model, J. Atmos. Ocean. Tech., 26, 22–32, doi:10.1175/2008JTECHA1134.1, 2009.

AMTD
7, 12219–12248, 2014

Table 1. Doppler lidar specifications.

Wavelength	1.5 µm
Pulse repetition rate	15 kHz
Nyquist velocity	20 m s^{-1}
Sampling frequency	50 MHz
Velocity resolution	0.038 m s^{-1}
Points per range gate	10
Range resolution	30 m
Pulse duration	0.2 µs
Lens diameter	33 µrad
Telescope	monostatic optic-fibre coupled

AMTD
7, 12219–12248, 2014

Table 2. Scan settings at Limassol and Loviisa. At Loviisa the 15° elevation angle VAD integration time was decreased from 10 to 7 s on 11 February 2014.

Site	Limassol		Loviisa	
VAD elevation angle [°]	10	30	4	15
Number of azimuthal angles	23	24	72	24
Integration time [s]	3	3	7	10/7
Repeat interval [min]	20	20	30	15

AMTD
7, 12219–12248, 2014

Table 3. Comparison of VAD and vertically-pointing mixing height estimate. The comparison is performed for cases when vertical measurements indicate mixing height is at the top of the lowest gate. The median VAD-based mixing height estimate is indicated in bold; upper and lower quartiles for VAD-based mixing height estimates are also indicated. For the 4° elevation angle, the VAD reference mixing height is taken from the lowest level of the 15° elevation angle VAD.

VAD elevation angle	VAD mixing height [m a.s.l.] percentile			*N*	VAD radius	Reference mixing height
[°]	25th	**50th**	75th		[m]	[m a.s.l.]
30	105	**150**	195	95	182	120
10	94	**145**	171	119	595	120
15	170	**187**	230	33	504	159
4	47	**50**	53	26	444	55

AMTD
7, 12219–12248, 2014

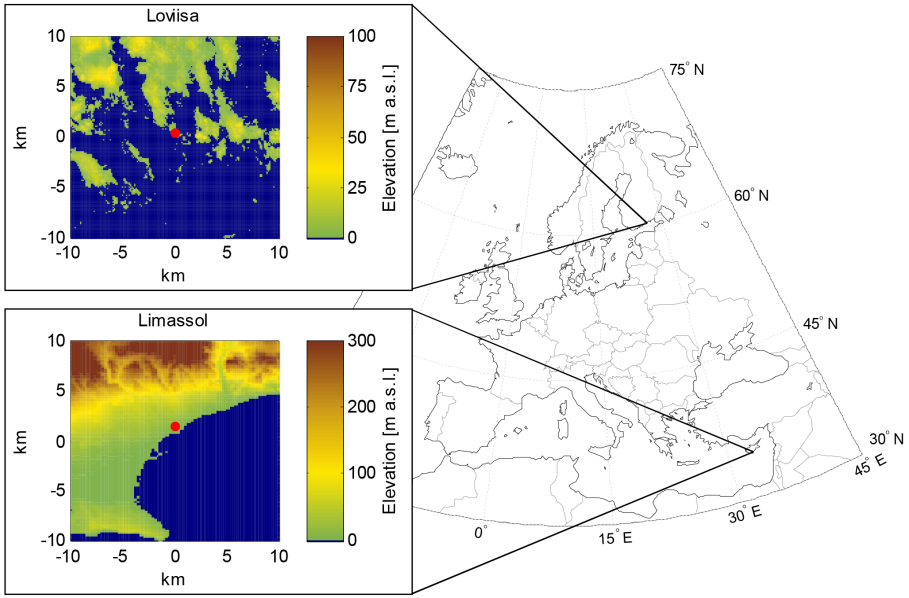

Figure 1. Location of Loviisa and Limassol measurement sites. In the 20 km × 20 km topographic map inserts for Loviisa (National Land Survey of Finland, 2014) and Limassol (United States Geological Survey, 2014) the location of the lidar is indicated by a red dot.

AMTD
7, 12219–12248, 2014

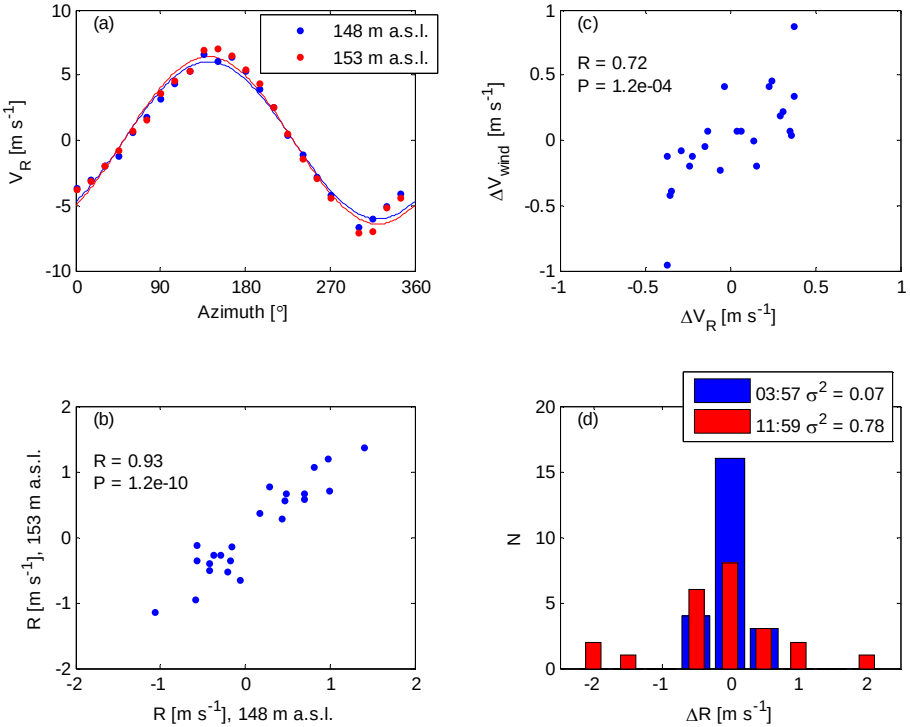

Figure 2. (a) Radial wind speed and sinusoidal fit on 24 August 2013 at 03:57 (UTC) for two consecutive altitudes from a 10° elevation angle VAD scan. **(b)** Scatterplot of the residuals of the fit presented in panel **(a)**. **(c)** The radial velocity change from the sinusoidal fits presented in **(a)** plotted against the observed radial velocity change with height (Eq. 3). **(d)** Histogram of the difference of residuals at 148 and 153 m a.s.l. altitudes from a 10° elevation angle VAD scan for a calm period (03:57 UTC) and a turbulent period (11:59 UTC) with corresponding variances indicated in the legend. The σ_v^2 (Eq. 10) is 0.03 at 03:57 UTC and 0.04 at 11:59 UTC, respectively.

AMTD
7, 12219–12248, 2014

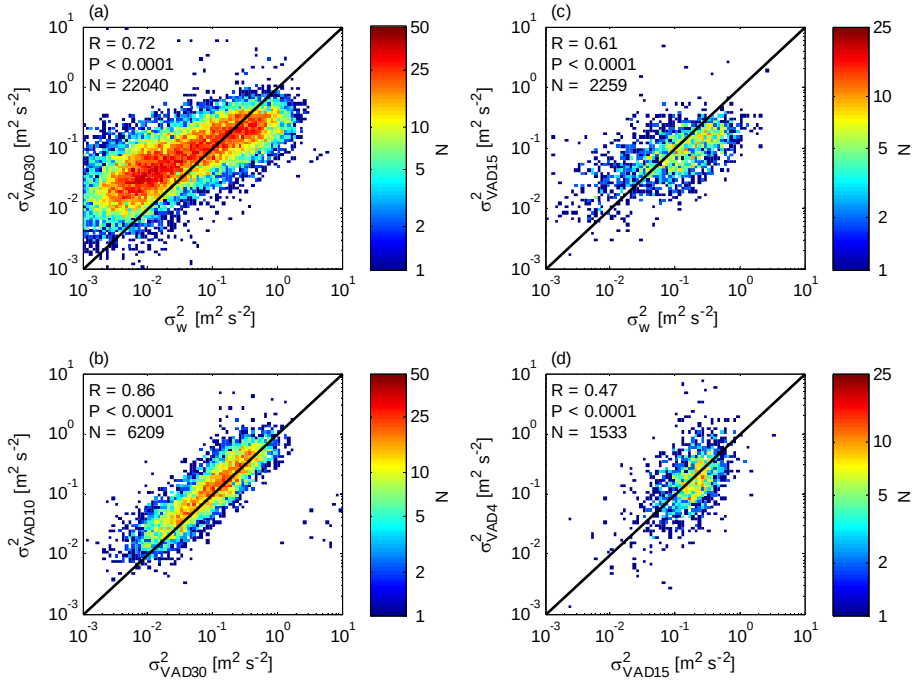

Figure 3. Frequency plots of **(a)** σ^2_{VAD} vs. σ^2_w for 30° elevation angle VAD at Limassol, **(b)** σ^2_{VAD} from 10° elevation angle VAD vs. σ^2_{VAD} from 30° elevation angle VAD at Limassol, **(c)** σ^2_{VAD} vs. σ^2_w for 15° elevation angle VAD at Loviisa and **(d)** σ^2_{VAD} from 4° elevation angle VAD vs. σ^2_{VAD} from 15° elevation angle VAD at Loviisa. Only VAD measurements for radius < 500 m are included. The σ^2_v contribution (Eq. 10) has been subtracted from σ^2_w. Correlation coefficient for logarithmic data and 1 : 1 line are included in all plots.

AMTD
7, 12219–12248, 2014

Low-level mixing height detection in coastal locations with a scanning Doppler lidar

V. Vakkari et al.

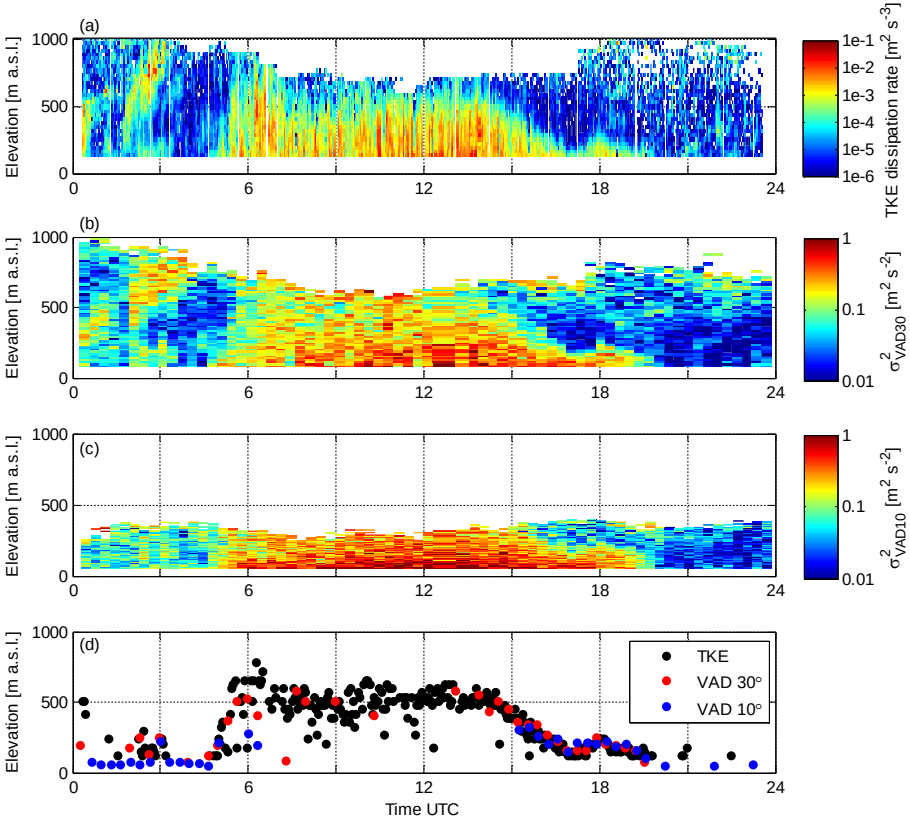

Figure 4. Diurnal variation of **(a)** TKE dissipation rate, **(b)** σ^2_{VAD} from 30° elevation angle VAD, **(c)** σ^2_{VAD} from 10° elevation angle VAD, and **(d)** mixing height, at Limassol on 24 August 2013.

AMTD
7, 12219–12248, 2014

Low-level mixing height detection in coastal locations with a scanning Doppler lidar

V. Vakkari et al.

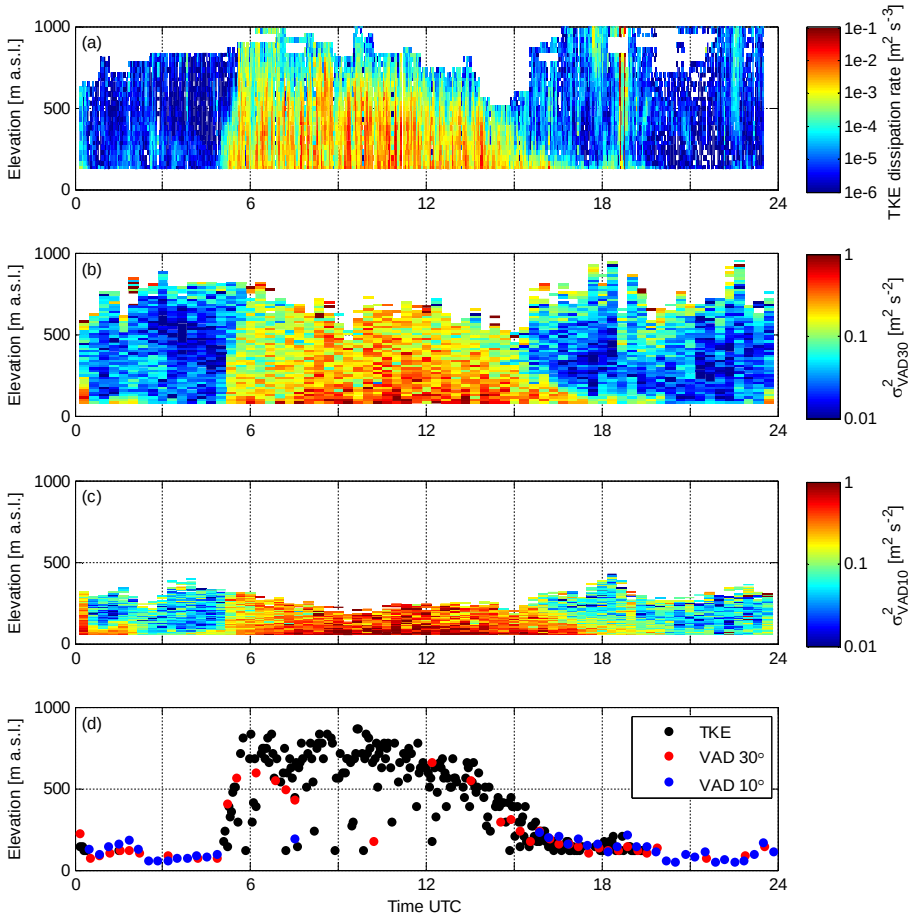

Figure 5. Diurnal variation of **(a)** TKE dissipation rate, **(b)** σ^2_{VAD} from 30° elevation angle VAD, **(c)** σ^2_{VAD} from 10° elevation angle VAD, and **(d)** mixing height, at Limassol on 17 September 2013.

AMTD
7, 12219–12248, 2014

Low-level mixing height detection in coastal locations with a scanning Doppler lidar

V. Vakkari et al.

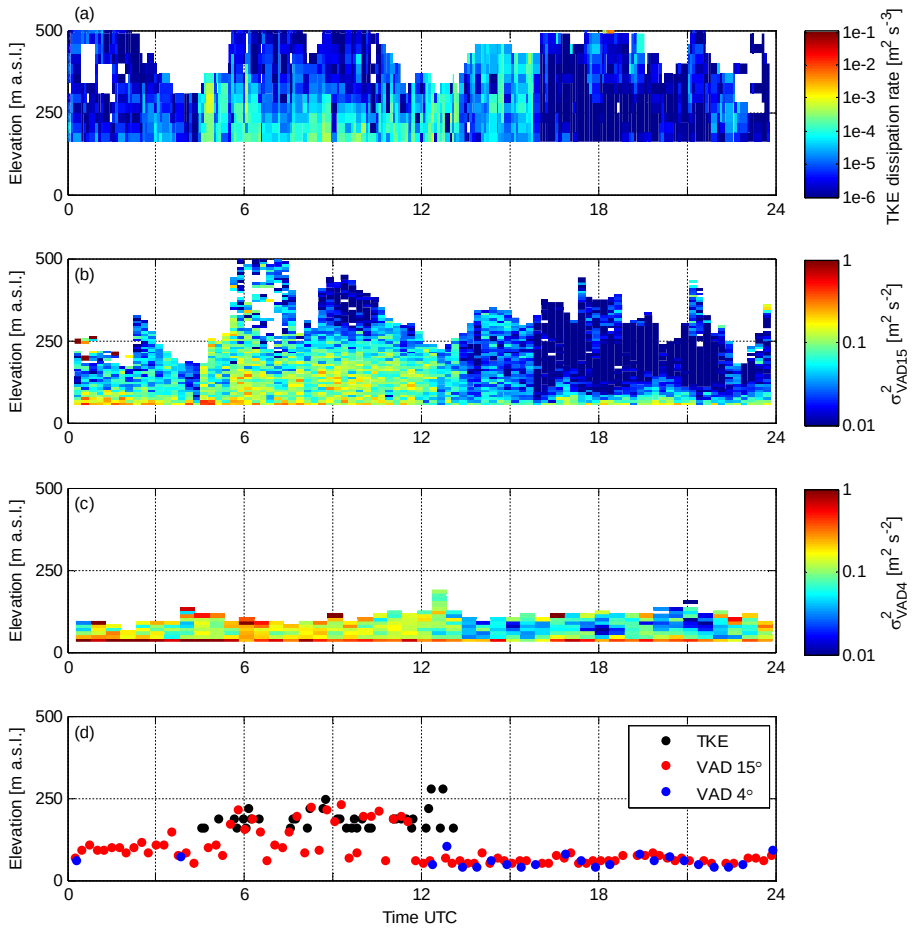

Figure 6. Diurnal variation of **(a)** TKE dissipation rate, **(b)** σ^2_{VAD} from 15° elevation angle VAD, **(c)** σ^2_{VAD} from 4° elevation angle VAD, and **(d)** mixing height, at Loviisa on 26 December 2013.

AMTD
7, 12219–12248, 2014

Low-level mixing height detection in coastal locations with a scanning Doppler lidar

V. Vakkari et al.

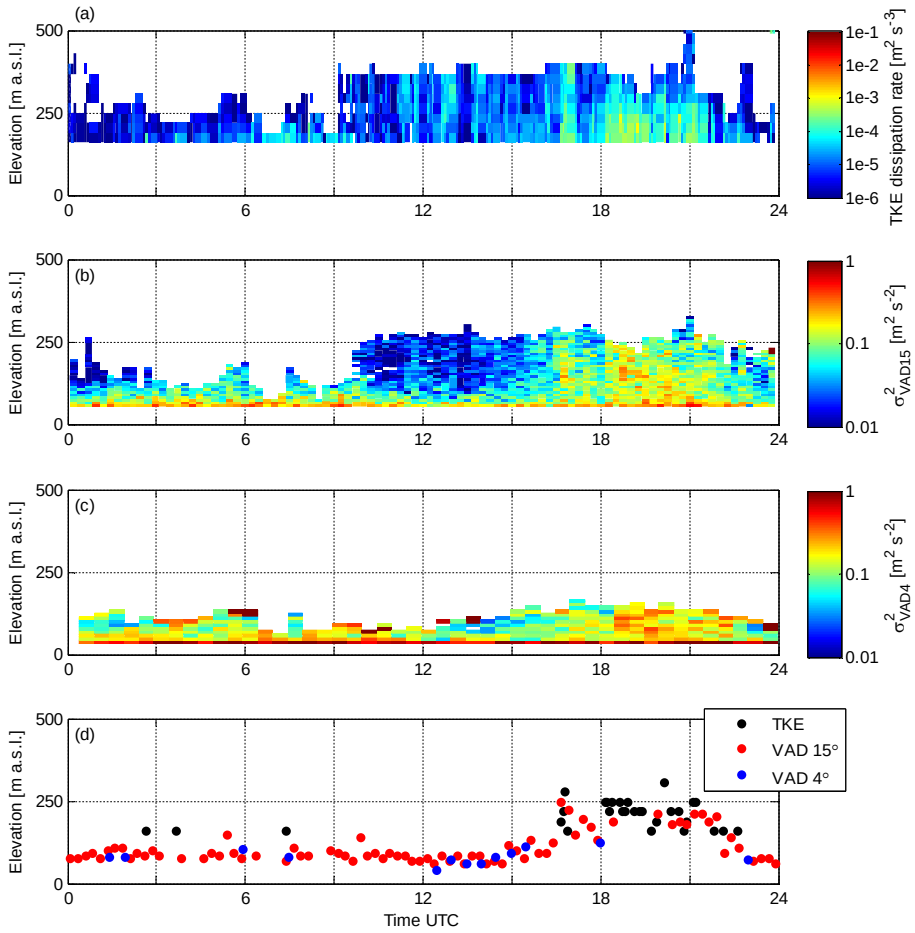

Figure 7. Diurnal variation of **(a)** TKE dissipation rate, **(b)** σ^2_{VAD} from 15° elevation angle VAD, **(c)** σ^2_{VAD} from 4° elevation angle VAD, and **(d)** mixing height, at Loviisa on 27 December 2013.

AMTD
7, 12219–12248, 2014

Low-level mixing height detection in coastal locations with a scanning Doppler lidar

V. Vakkari et al.

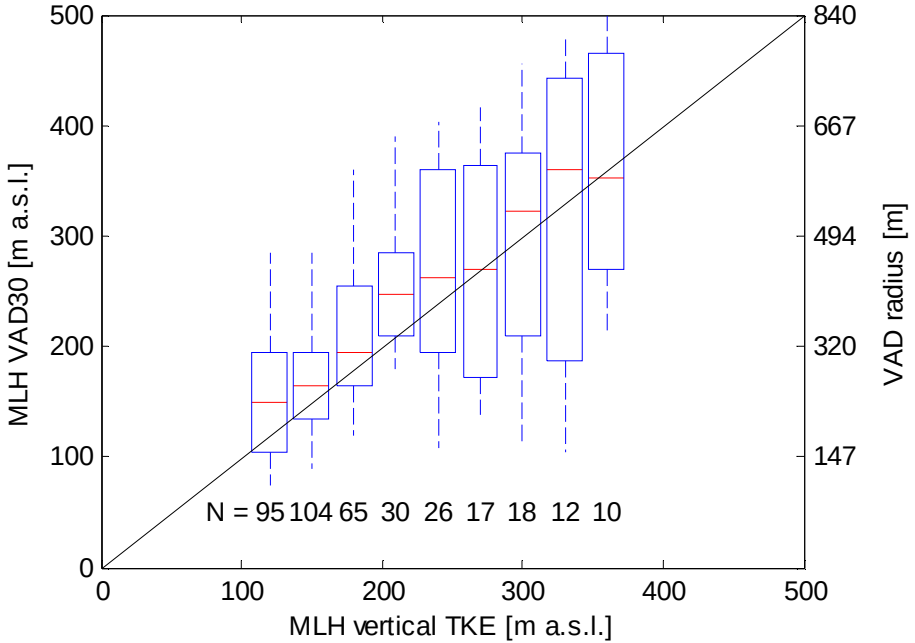

Figure 8. Comparison of vertical TKE dissipation rate based mixing height estimate and σ^2_{VAD} based mixing height for 30° elevation angle VAD at Limassol. Red line indicates median, blue rectangle indicates upper and lower quartiles and whiskers indicate the 10th and 90th percentile. Black line indicates 1 : 1 line. The right hand side axis indicates the radius of the VAD corresponding to the elevation on left hand side axis.

AMTD
7, 12219–12248, 2014

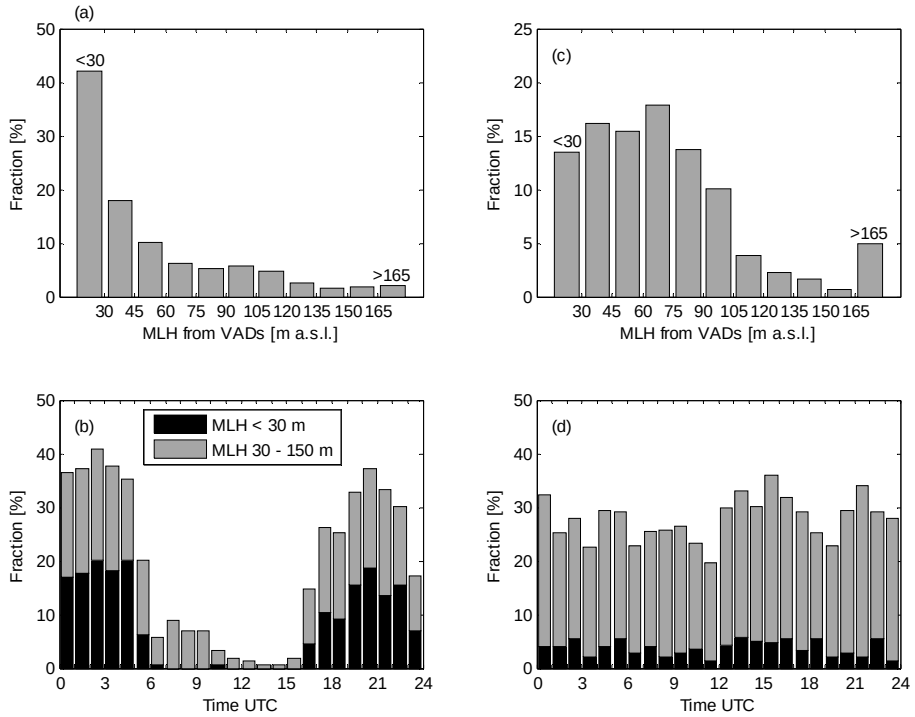

Figure 9. Histogram of mixing height derived from VADs for the cases when vertical measurements indicate mixing height to be below minimum range at vertical for Limassol **(a)** and Loviisa **(c)**. The minimum range for mixing height calculation from vertical measurements was 120 m a.s.l. at Limassol and 159 m a.s.l. at Loviisa, respectively. **(b)** Diurnal frequency of low mixing heights at Limassol. **(d)** Diurnal frequency of low mixing heights at Loviisa. The minimum range for mixing height calculation from VADs was 30 m a.s.l. at both Limassol and Loviisa.

AMTD
7, 12219–12248, 2014

Low-level mixing height detection in coastal locations with a scanning Doppler lidar

V. Vakkari et al.